RSC Advances

PAPER

View Article Online
View Journal | View Issue

Cite this: *RSC Adv.*, 2014, **4**, 52583

Nitrogen-doped graphene quantum dots-based fluorescent probe for the sensitive turn-on detection of glutathione and its cellular imaging†

Jian Ju,[a] Ruizhong Zhang,[ab] Shuijian He[ab] and Wei Chen*[a]

Received 17th September 2014
Accepted 15th October 2014

DOI: 10.1039/c4ra10601f

www.rsc.org/advances

In this paper, highly blue-luminescent nitrogen-doped graphene quantum dots (N-GQDs) are synthesized by a facile one-step hydrothermal treatment of citric acid and dicyandiamide. A quantum yield (QY) as high as 32.4% is achieved at an excitation wavelength of 350 nm. It is found that such N-GQDs with a high QY can be used as efficient fluorescent probes for the detection of glutathione (GSH). In the detection, the photoluminescence (PL) intensity of the N-GQDs could be quenched by mercuric ions due to the strong electrostatic interaction and electron transfer between N-GQDs and Hg(II). Upon the addition of GSH, the PL intensity of N-GQDs can be recovered owing to the preferred combination of Hg(II) and GSH by forming a Hg(II)–S bond. Under optimal conditions, this fluorescence turn-on sensing system exhibits excellent sensitivity and selectivity for GSH determination with a detection limit of 87 nM. Importantly, the N-GQDs–Hg(II) system can be successfully applied for visualizing the intracellular GSH in live HeLa cells due to bright luminescence, low cytotoxicity and good biocompatibility.

1. Introduction

Glutathione (GSH) plays critical roles in many physiological processes usually present in live cells, such as reversible redox reactions inside cells and important cellular functions.[1–3] More importantly, the concentration levels of GSH have been implicated in a number of debilitating diseases such as AIDS, cancer and Alzheimer's disease.[4,5] Thus sensitive and selective detection of GSH is very important for the early diagnosis of these diseases.

Recently, great attention has been paid to fluorescent probes for detecting various biothiols, including cystein (Cys), homocystein (Hcy) and glutathione (GSH), owing to the advantages of high sensitivity, specificity and real-time determination.[6–8] Wang *et al.*[9] used CdTe quantum dots as probes for the fluorescent detection of biothiols based upon the competition effect between thymidine–thymidine mismatch and biothiols with Hg(II). In the absence of biothiols, the photoluminescence (PL) intensity of the fluorescent probes is very weak, due to the high quenching ability of Hg(II). However, the PL intensity of the fluorescent probes was recovered under the presence of biothiols, owing to the strong binding preference of biothiols to Hg(II). Some other similar works have also been studied, and various fluorescent probe materials, such as conjugated polymers,[10] fluorescent molecule probes,[11–14] noble metal nanoparticles,[2,15–17] colloid semiconductor quantum dots[5,9] and carbon dots[18,19] have been widely reported in the recent past. Among these reported fluorescent probes, carbon dots exhibited many advantages, such as low toxicity, high luminescence, and easy preparation.[20–22] Therefore, it is necessary and important to make further efforts to develop simple, efficient and inexpensive carbon-based materials for the fluorescent recognition of biothiols.

Graphene quantum dots (GQDs) have sparked significant excitement as a promising new class of carbon-based luminescent nanomaterials, owing to their tunable photoluminescence properties.[23,24] Recently, GQDs have been attracting increasing interest in the field of fluorescent biosensor and bioimaging due to their good biocompatibility and photostability. Tian's group designed a label-free fluorescence turn-on assay of trypsin using cytochrome c-induced GQDs.[25] Qu and co-workers used the Ag nanoparticle-decorated GQDs for sensitive detection of Ag^+ and biothiols.[19] This sensing platform exhibited excellent specificity of Ag^+ and biothiols. However, the QYs of the reported GQDs are much lower than the conventional semiconductor QDs, which largely limits their wide applications. Therefore, how to improve the QYs is one of the challenges for the application of GQDs. Recently, various studies have demonstrated that the electronic structure and fluorescence of GQDs can be effectively turned by doping hetero atoms to the π-conjugated system or amino-functionalized GQDs. Li

[a]*State Key Laboratory of Electroanalytical Chemistry, Changchun Institute of Applied Chemistry, Chinese Academy of Sciences, Changchun 130022, Jilin, China. E-mail: weichen@ciac.ac.cn*

[b]*University of Chinese Academy of Sciences, Beijing 100039, China*

† Electronic supplementary information (ESI) available: FTIR spectrum of the N-GQDs; UV-vis absorption spectra of the N-GQDs in PBS solution with and without 10 μM Hg(II); fluorescence intensity of N-GQDs in the presence of various metal ions; and PL intensity change of the N-GQDs–Hg(II) aqueous solution with time after addition of 30 μM GSH. See DOI: 10.1039/c4ra10601f

et al.[26] found that the as-prepared N-GQDs possess unique optoelectronic properties due to the strong electron-withdrawing effect of the doped nitrogen atom. Chattopadhyay's group proposed a possible mechanism for tuning the fluorescent properties of GQDs through the charge transfer effect of functional groups.[27] It can be expected that nitrogen-doped GQDs can be used to design practical biosensors for determination of GSH in live cells by tuning their surface structure and the related fluorescent properties. Meanwhile, N-GQDs usually exhibit larger quantum yield than GQDs, which is beneficial for fluorescence study in living cells. Although valuable, to the best of our knowledge, N-GQDs have not been utilized to date in the recognition of GSH in living cells.

Various methods have been developed for the preparation of nitrogen-doped GQDs. For instance, Li *et al.*[26] used chemical oxidation method for preparing N-doped GQDs. Hu *et al.* reported one-step preparation of N-GQDs from hydrothermal cutting graphene oxide.[28] Nevertheless, above methods are unsatisfactory due to the expensive equipment required, complicated and time-consuming procedures. In this work, we report a one-step, low-cost and environment-friendly strategy to prepare N-doped GQDs by hydrothermal treatment of citric acid and dicyandiamide (DCD). The obtained N-GQDs emit bright blue-luminescence with a high quantum yield (QY).

Herein, a new kind of fluorescent sensor for GSH detection was fabricated based on the fluorescence turn-on of the N-GQD–Hg(II) system. Due to the strong electrostatic interaction and electron transfer between N-GQDs and Hg(II), the PL intensity of the N-GQDs could be quenched efficiently by Hg(II). However, with the presence of GSH, the PL intensity of the N-GQDs can be recovered due to the release of Hg(II) from the surface of N-GQDs by forming the strong Hg(II)–S bond. Based on this, the N-GQDs fluorescent probe offers high sensitivity and excellent specificity for GSH detection. More importantly, the N-GQDs–Hg(II) system can be applied for visualizing the intracellular GSH level in living cancer cells.

2. Experimental

2.1 Chemicals

Citric acid (CA), dicyandiamide (DCD), NaH_2PO_4 and Na_2HPO_4 were purchased from Beijing Chemical Reagent Co., China. *N*-Ethylmaleimide, cystein (Cys), homocystein (Hcy) and glutathione (GSH) were purchased from Aladin Ltd. (Shanghai, China). Dulbecco's modified eagle medium (DMEM), penicillin, fetal bovine serum (FBS), and streptomycin were purchased from Beijing Dingguo Biotechnology Co. All Reagents are of analytical grade and used as received. The 0.1 M phosphate buffer solution (PBS) was prepared by mixing 19 mL of 0.1 M NaH_2PO_4 and 81 mL of 0.1 M Na_2HPO_4. PBS buffer used in cell culture was purchased from Invitrogen (10010). Nanopure water (18.3 MΩ cm) was used throughout the experiments.

2.2 Characterizations

The morphology and structure of the as-synthesized N-GQDs were characterized by high resolution transmission electron microscopy (HRTEM, FEI TECNAI F20 EM). Atomic force microscope (AFM) images were acquired using a Multimode Nanoscope V scanning probe microscopy system (Bruker, USA). XPS measurements were performed on a Thermo ESCALAB VG Scientific 250 spectrometer equipped with monochromatized Al Kα excitation. FT-IR spectra were recorded using the KBr pellet method (VERTEX70). Fluorescence spectra were measured by using a Perkin-Elmer LS-55 Luminescence Spectrometer (Perkin-Elmer Instruments, UK). UV-vis absorption spectra were measured on a UV-1700 (MAPADA, China) spectrometer with a 1 cm quartz cuvette. The cells were imaged using a confocal laser scanning fluorescence microscopy (CLSM, Leica TCS SP2, Leica Microsystems, Mannheim, Germany).

2.3 Preparation of N-GQDs

N-GQDs were prepared here by hydrothermal treatment of citric acid (CA) and dicyandiamide. In a typical synthesis, 2 g CA and 1 g DCD were mixed with nanopure water (5 mL). The mixture was then transferred into a 25 mL Teflon lined autoclave and heated at 180 °C for 12 h. After the reaction, the reactor was cooled down to room temperature naturally. The product was transferred to 100 mL nanopure water; the concentration and pH of the N-GQDs aqueous solution are about 20 mg mL^{-1} and 7.0, respectively. Then 30 μL N-GQDs (20 mg mL^{-1}) were dispersed in 100 mL PBS as stock solution (6 μg mL^{-1}) for further characterization and use.

2.4 Quantum yields (QYs) measurements

QYs of the GQDs and N-GQDs were determined by using quinine sulphate (QY = 0.54 in water) as the standard sample, and were calculated according to the following equation:[29]

$$Q_x = Q_{st}\frac{I_x}{I_{st}}\frac{A_{st}}{A_x}\frac{n_x^2}{n_{st}^2} \quad (1)$$

where Q is the quantum yield, I is the measured integrated emission intensity, n is the refractive index, and A is the extinction. The subscript "st" refers to the standard with known QY and "x" for sample.

2.5 Fluorescence measurements

All the fluorescence detections were conducted under the same conditions and the excitation wavelength was set at 350 nm. First, 3 mL PBS solution of N-GQDs (6 μg mL^{-1}) was added in a quartz cuvette, followed by the addition of a certain volume of Hg(II) solution. GSH was then added to the above mixed solution. The PL spectra of the mixed solutions were recorded and all experiments were performed at room temperature. It should be pointed out that PBS is a kind of common buffer solution with a wide range of pH regulation which can be used to simulate human biological environment. Here, in order to examine the practical application of fluorescent N-GQD–Hg(II) system for sensing GSH in living cell, PBS solution is used as the media solution.

2.6 Cell culture and viability measurements

HeLa cells were cultured in a DMEM medium containing 10% fetal bovine serum (FBS) supplemented with 100 units per mL penicillin and 100 mg mL^{-1} streptomycin in an incubator at 37 °C with 5% CO_2.[29,30] Cell viability was measured using a standard MTT assay. HeLa cells were seeded in a 96-well plate at a density of 1×10^4 cell per well and then incubated with different concentrations of N-GQDs and N-GQDs–Hg(II) (0.625–20 μg mL^{-1}) dispersed in the DMEM medium for 24 h.

The incubation solution was removed and washed with PBS for three times. The MTT solution (100 μL, 0.5 mg mL^{-1}) was added to each well and incubated for 4 h. Finally, the medium was replaced with 100 μL of DMSO, and the absorbance was read at 570 nm using a Versamaxmicroplate reader (BioTek Instruments Inc, USA).[31] Results were quantified by manually subtracting the blank value and normalized against the control values.

2.7 Confocal fluorescence imaging analysis

HeLa cells were plated at a density of 5.0×10^5 cells per dish on glass bottom cell culture dishes (20 mm) at 37 °C in a humidified atmosphere containing 5% CO_2 for 24 h. The cells were washed with PBS (purchased from Invitrogen) for three times, followed by incubation with 800 μL of N-GQDs–Hg(II) (6 μg mL^{-1}) in DMEM culture medium at 37 °C and 5% CO_2 for 2 h. After incubation was completed, the resulting cells were washed three times with PBS. The cells were imaged using a confocal laser scanning fluorescence microscopy with 20× objective with excitation wavelength at 488 nm and observed through a 500–550 nm emission band-pass.

3. Results and discussion

3.1 Characterization of the as-synthesized N-GQDs

First, the morphology of the as-prepared N-GQDs was characterized by AFM and TEM. The AFM image (Fig. 1A) reveals that well-dispersed quantum dots were produced and a typical topographic height of 0.5–1.5 nm can be measured from the height profile. Considering the theoretical thickness of a graphene monolayer of 0.34 nm, the AFM data imply that most of the N-GQDs consist of 1–5 graphene layers. Fig. 1B shows the TEM image of the N-GQDs, from which it can be seen that the formed N-GQDs are small sheets with a narrow size distribution. From the size histogram shown in Fig. 1C, the average diameter of the N-GQDs is 3.8 nm, as judged from image analysis of 100 individual particles. Compared to the GQDs reported previously (0.5–2 nm in thickness and ~15 nm in diameter),[32] our synthesized N-GQDs exhibit the similar height but much smaller lateral size. Fig. 1D shows the high resolution TEM (HRTEM) image of the N-GQDs. It can be seen that the quantum dots prepared with the present method show high crystallinity with a clear lattice spacing of 0.23 nm, corresponding to (1 1 $\bar{2}$ 0) lattice fringes of graphene.[33,34]

The surface chemistry of the N-GQDs was also identified by FTIR spectroscopy. The FTIR spectrum (Fig. S1†) shows the absorption of stretching vibration of C–O at 1100 cm^{-1}, C–H stretching vibration below 1350 cm^{-1}, and the broad O–H stretching peak at 3402 cm^{-1}. In addition, the absorption peaks at 1380, 1650 and 3200 cm^{-1} can be observed, corresponding to the C–N, NH–CO and N–H stretching absorption, respectively.[33,34]

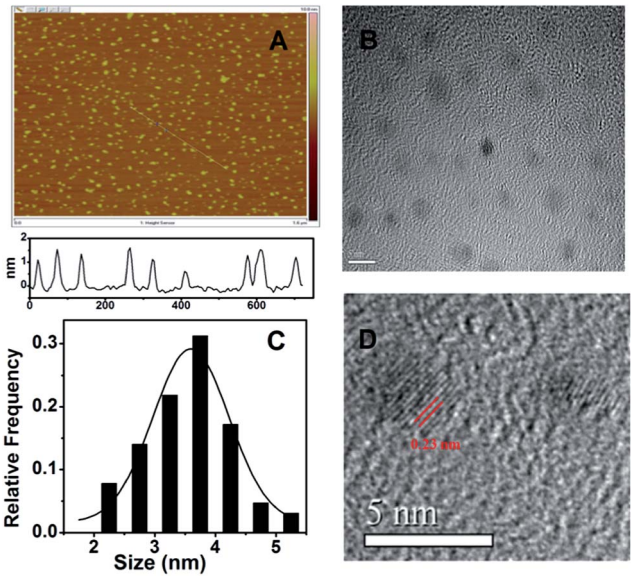

Fig. 1 (A) AFM image of the N-GQDs on a mica substrate with the height profile along the line shown in the image. TEM image (B), the size distribution histogram (C) and HRTEM image (D) of the as-synthesized N-GQDs.

Fig. 2A shows the schematic illustration of the preparation process of the N-GQDs. According to the previous studies, graphene quantum dots can be formed by direct carbonizing citric

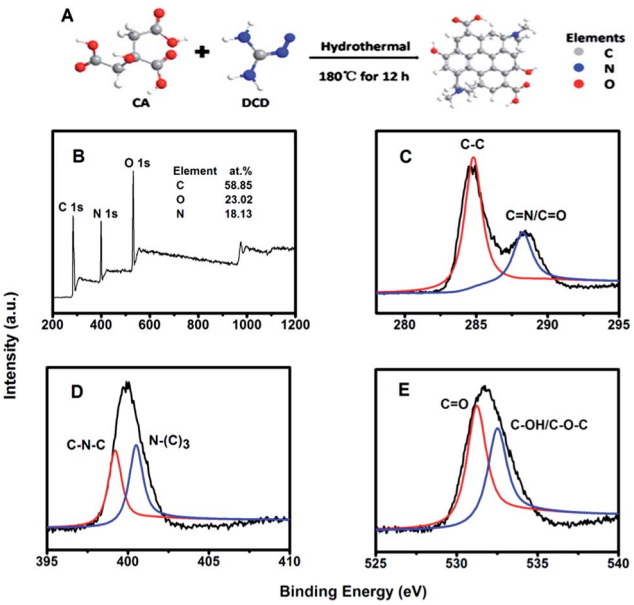

Fig. 2 (A) Scheme of the preparation of N-GQDs by a hydrothermal process. (B) XPS survey spectra of the N-GQDs; XPS spectra of C1s (C), N1s (D) and O1s (E) of the N-GQDs.

acid at a certain temperature. Here, during the pyrolyzing process, dicyandiamide was added as nitrogen source. We found that after hydrothermal process at 180 ° C for 12 h, N-doped GQDs could be obtained. The composition of the produced N-GQDs was then characterized by X-ray photoelectron spectroscopy (XPS). The survey spectrum (Fig. 2B) of the N-GQDs clearly shows the presence of C, O and N. The three predominant peaks at 284.0, 400.0, and 530.6 eV can be assigned to C1s, N1s, and O1s, respectively. The doping concentration of nitrogen was calculated to be 18.13%, which is much higher than those reported before with other methods and precursors.[26,28,35] Such result implies that the N-GQDs with high doping concentration of nitrogen can be synthesized by using DCD as nitrogen-containing precursor. The two peaks at 284.6 and 288.1 eV in the C1s photoelectron spectrum (Fig. 2C) could be assigned to the binding energy of carbon in C–C, and C=N/C=O, respectively. In the high-resolution N1s spectrum (Fig. 2D), the two peaks at 399.2 and 400.5 eV can be assigned to C–N–C and N–$(C)_3$ bonds, respectively. From the O1s spectrum shown in Fig. 2E, two fitted peaks at 531.7 and 533.0 eV are assigned to C=O and C–OH/C–O–C groups, respectively. The XPS analyses clearly demonstrate that nitrogen atoms have been successfully doped into the framework of GQDs.[35,36]

Fig. 3A shows the UV-vis absorption and PL emission spectra of the N-GQDs dispersed in PBS solution. For the N-GQDs, a typical absorption peak at *ca.* 230 nm was observed, which is assigned to the π–π* transition of aromatic C=C sp^2 domains. Another strong absorption peak at 330 nm can be regarded as the n–π* transition of the C=O bone, which can result in strong fluorescence.[37,38] As shown in Fig. 3A, the N-GQDs exhibited a maximum emission at 440 nm with an excitation wavelength of 350 nm. Compared to the non-doped GQDs,[32,35] the present N-GQDs show blue-shifted emission, which could be ascribed to the strong electron affinity of the doped nitrogen.[26] It should be noted that the excitation peak is very close to the absorption peak, suggesting the high-efficient emitting absorption of the N-GQDs. With quinine as a reference and based on eqn (1), the quantum yield (QY) of the as-prepared N-GQDs was calculated to be 32.4% at an excitation wavelength of 350 nm. From the photographs shown in Fig. 3A inset, the high QY leads to the intense bright blue emission from the solution of N-GQDs under excitation with a 365 nm UV light. Fig. 3B shows the emission spectra of the N-GQDs under different excitation wavelengths. It can be seen that the emission peak shows red-shift from 438 to 475 nm by increasing the excitation wavelength from 320 to 420 nm. Such phenomenon has also been observed from other carbon-based quantum dots, which may arise from the different particle size and different emission sites of the formed N-GQDs.[24,39,40]

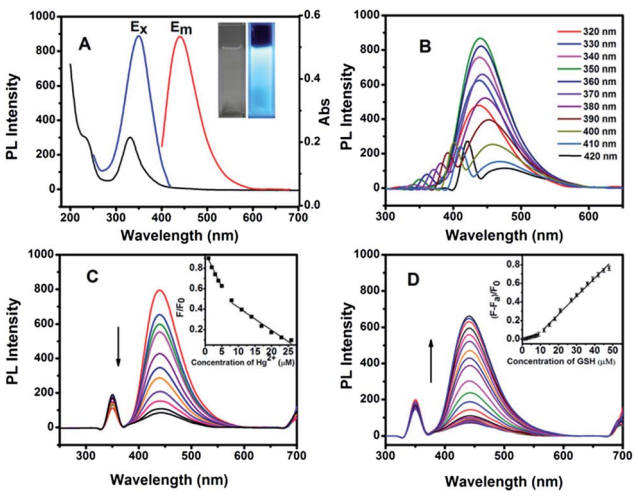

Fig. 3 (A) UV-vis absorption, photoluminescence excitation (λ_{em} = 440 nm) and emission (λ_{ex} = 350 nm) spectra of the N-GQDs in PBS solution. Inset: photographs taken without (left) and with (right) UV lamp irradiation (365 nm). (B) Normalized PL spectra of the N-GQDs at different excitation wavelength. (C) Fluorescence emission spectra of the N-GQDs in 0.1 mol L^{-1} PBS solution upon addition of various concentrations of Hg(II) (form 0 to 23 μM). Inset shows the dependence of F/F_0 on the concentration of Hg^{2+} ions within the range of 0–23 μM. (D) FL emission spectra of the N-GQDs containing 10 μM Hg(II) with increasing the concentration of GSH, inset shows the relationship between fluorescence intensity of the N-GQDs and the concentration of added GSH.

As observed before, the fluorescence of the N-GQDs can be quenched efficiently by Hg(II). Fig. 3C displays the typical fluorescence spectra of the N-GQDs upon addition of different concentrations of Hg(II) at λ_{ex} = 350 nm. Fig. 3C inset indicates that two linear calibration plots can be fitted between the fluorescence intensity and the concentration of Hg(II) at the range from 0 to 23 μM. The quenching effect from Hg(II) can be ascribed to the interaction between N-GQDs–Hg(II). Fig. S2† show the UV-vis spectra of the N-GQDs in PBS solution with absence and presence of Hg(II). Upon the addition of 10 μM Hg(II), the absorption of N-GQDs centered at 230 nm disappeared, and the absorption at 330 nm became weaker. The UV-vis absorption change indirectly demonstrates that the fluorescence of N-GQDs can be quenched by Hg(II) ions due to the strong electrostatic interaction and electron transfer between N-GQDs and Hg(II). Our studies also showed that other metal ions have only a slight quenching effect on the fluorescence of N-GQDs (Fig. S3†). Therefore, the fluorescence of N-GQDs has a high selectivity to Hg(II) ions.

3.2 Detection of glutathione (GSH) by the fluorescence turn-on of the N-GQDs–Hg(II) system

Since the previous studies indicated that Hg(II) has a high affinity to thiol-containing GSH, their strong coordination could recover the quenched fluorescence emission of the N-GQDs–Hg(II) system, as shown in Scheme 1. Such fluorescence turn-on sensing system can be used for sensitive and selective detection of GSH. It should be noted that besides the enhanced quantum yield by N doping in GQDs, the previous study showed that the functional groups containing N and O in N-GQDs may improve their ability of chelation with metal irons, leading to efficient fluorescence quenching.[36] The proposed mechanism of GSH detection in this study is illustrated in Scheme 1. The sensing process includes two steps: the fluorescence quenching of the N-GQDs by forming N-GQDs–Hg(II) and the fluorescence turn-

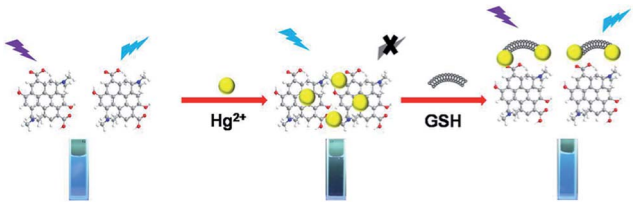

Scheme 1 Schematic illustration of the mechanism for fluorescence turn-on detection of glutathione (GSH) based on nitrogen-doped graphene quantum dots (N-GQDs).

on with the presence of GSH. By measuring the intensity of the recovered fluorescence, the concentration of GSH in the solution can be determined. We first investigated the required time for reaction equilibrium between N-GQDs–Hg(II) and GSH. Fig. S4† shows the intensity change of the PL spectra with time after addition of 30 μM GSH. It can be seen that the PL intensity exhibits almost no change after 3 min. Therefore, in the present study, each emission spectrum was collected after 3 min of mixing the N-GQDs–Hg(II) and GSH. Fig. 3D shows the fluorescence intensity of the N-GQDs containing 10 μM Hg(II) upon addition of different concentrations of GSH. For the original solution, there is a very weak emission at 440 nm due to the quenching effect from Hg(II). Clearly, with the addition of GSH, the fluorescence is recovered gradually and the emission intensity increases with increasing the GSH concentration. Fig. 3D inset displays good linear relationship between $(F - F_a)/F_0$ and the GSH concentration from 0.5 to 48 μM. The linear fitting could be described by two equations: $y = 0.061x - 0.00693$ ($R = 0.993$, for concentrations of 0.5–9 μM) and $y = 0.019x - 0.114$ ($R = 0.992$, for concentrations of 9–48 μM). Here, F_0 is the PL intensity of the N-GQDs solution at 440 nm, F_a is the fluorescence intensity of the N-GQDs containing 10 μM Hg(II) and F is the recovered fluorescence intensity of N-GQDs in the presence of GSH. The detection limit is estimated to be 87 nM at a signal-to-noise ratio of 3, which is much lower than those of the previously reported fluorescence probes.[9,41,42]

3.3 Selectivity of the N-GQDs–Hg(II) system towards GSH detection

To evaluate the selectivity of the sensor for GSH detection, the fluorescence responses to the other amino acids at the same concentration were also investigated. As shown in Fig. 4, Cys, Hcy and GSH exhibit significant turn-on effect on the fluorescence intensity of the N-GQDs–Hg(II). The restoration ability follows the order of GSH > Cys > Hcy. Moreover, the recovery efficiency of GSH is significantly higher than those of other amino acids. It should be pointed out that although Cys and Hcy can also turn on the quenched fluorescence, the intracellular level of GSH in mammalian cells is higher than Cys and Hcy. Hence, the N-GQDs–Hg(II) could be a promising sensing platform for detecting the intracellular GSH with high selectivity.

In addition, the prominent fluorescence color change of N-QGDs–Hg(II) upon addition of amino acids can be distinctly

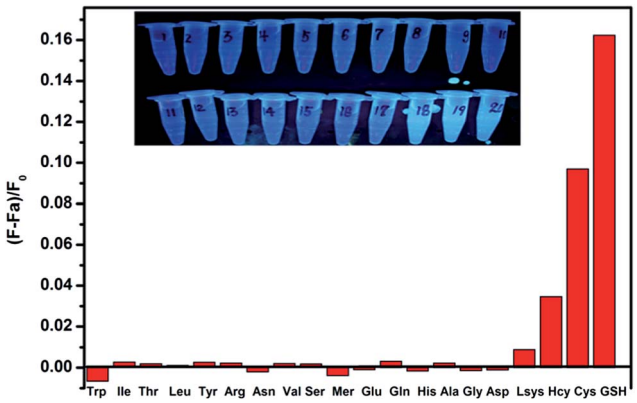

Fig. 4 Fluorescence emission intensity of the N-GQDs–Hg(II) upon addition of different kinds of amino acids. [Hg^{2+}] = 20 μM, [amino acids] = 10 μM. Inset shows the fluorescent color of the N-GQDs–Hg(II) complex after adding different kinds of amino acids under UV light (λ_{ex} = 365 nm).

observed by the naked eye under UV lamp. Fig. 4 inset shows the fluorescence color of the N-GQDs–Hg(II) complex with addition of different amino acids under UV light (λ_{ex} = 365 nm). Among the studied twenty kinds of natural amino acids, only the N-GQDs–Hg(II) solutions containing Cys, Hcy and GSH display a bright blue fluorescence color under UV light. These results indicate again that the N-GQDs–Hg(II) system has a high selectivity for GHS detection even with the presence of other amino acids.

3.4 Application of the fluorescent N-GQDs in bioimaging

The N-GQDs–Hg(II) can be used to visualize the GSH in living cell. Here, we carried out an *in vitro* bioimaging study with human cervical carcinoma HeLa cells by scanning confocal microscopy. The HeLa cells were first incubated with the DMEM culture medium at 37 °C and 5% CO_2 for 24 h. Then living HeLa cells were incubated with the N-GQDs–Hg(II) (6 and 2 μg mL^{-1}

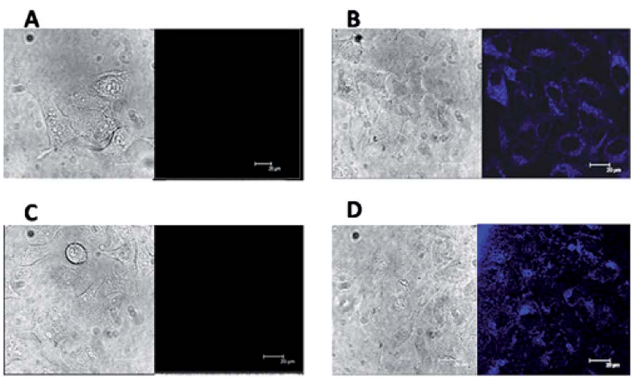

Fig. 5 Scanning confocal microscopy images of (A) HeLa cells and (B) HeLa Cells incubated with the N-GQDs–Hg, (C) after pre-treated with *N*-ethylmaleimide (0.5 mM), HeLa cells incubated with the N-GQDs–Hg(II), (D) HeLa cells were pre-treated with 200 μM GSH and then incubated with N-GQDs–Hg(II). Incubation was carried out at 37 °C for 2 h.

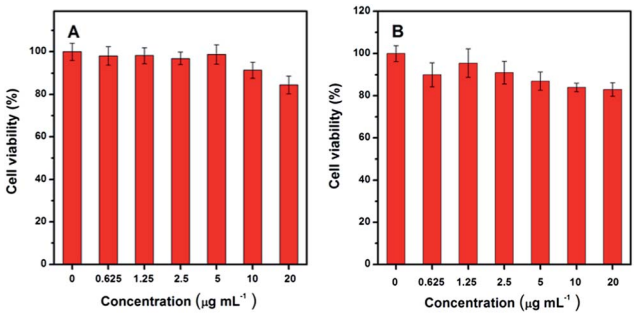

Fig. 6 Relative viabilities of HeLa cells after incubated for 24 h with different concentrations of N-GQDs (A) and N-GQDs–Hg(II) (B).

for N-GQDs and Hg(II), respectively) in DMEM culture medium for another 2 h. From Fig. 5A, no fluorescence signal was observed for HeLa cells without the incubation of nanocomposites in control group with excitation at 488 nm. However, a bright blue fluorescence emission could be observed for the cells incubated with the N-GQDs–Hg(II) (Fig. 5B). In another control group shown in Fig. 5C, upon addition of 0.5 mM *N*-ethylmaleimide for 30 min to consume all free thiols in HeLa cells, no significant fluorescence signal was observed.[17] In addition, if the HeLa cells were added and incubated with 200 μM GSH for 2 h, much stronger blue fluorescence signal (Fig. 5D) can be observed compared with that shown in Fig. 5B. Therefore, the uptake of N-GQDs–Hg(II) into the HeLa cells occurred, and the fluorescence change is really dependent on the concentration of the intracellular GSH level. Thus, the N-GQDs–Hg(II) "turn-on" system might provide a simple way to monitor the intracellular GSH level.

The toxicity of materials is crucial for their biomedical applications. To evaluate the toxicity of the N-GQDs containing Hg(II), MTT assays were performed on HeLa cell lines. As shown in Fig. 6, these cell lines still retain high cell viabilities greater than 85% even after 24 h of treatment with either N-GQDs or N-GQDs–Hg(II) with concentration up to 20 μg mL^{-1}. These results indicate that the N-GQDs and N-GQDs–Hg(II) have low cytotoxicity and good biocompatibility.

4. Conclusion

In this paper, we report a simple, low-cost and environmentally friendly synthetic strategy to prepare nitrogen-doped graphene quantum dots (N-GQDs). Through a facile one-step hydrothermal treatment, the as-prepared N-GQDs exhibited strong blue luminescence with a maximum quantum yield of 32.4%. It was found that the fluorescence of the N-GQDs can be efficiently quenched by Hg(II). On the other hand, due to the strong interaction between GSH and Hg(II), the fluorescence of the N-GQDs–Hg(II) can be recovered with the presence of GSH. Based on the dependence of the recovered fluorescence intensity on GSH concentration, this fluorescence turn-on sensor has been successfully applied to the sensitive and selective detection of GSH with a detection limit of 87 nM. With the excellent sensing performance, low toxicity and easy labeling, the as-prepared N-GQDs have promising applications in biological imaging, disease diagnosis and biosensor.

Acknowledgements

This work was supported by the National Natural Science Foundation of China (no. 21275136) and the Natural Science Foundation of Jilin province, China (no. 201215090).

Notes and references

1 O. Rusin, N. N. St Luce, R. A. Agbaria, J. O. Escobedo, S. Jiang, I. M. Warner, F. B. Dawan, K. Lian and R. M. Strongin, *J. Am. Chem. Soc.*, 2004, **126**, 438.
2 L. Shang, C. J. Qin, T. Wang, M. Wang, L. X. Wang and S. J. Dong, *J. Phys. Chem. C*, 2007, **111**, 13414.
3 W. H. Wang, J. O. Escobedo, C. M. Lawrence and R. M. Strongin, *J. Am. Chem. Soc.*, 2004, **126**, 3400.
4 J. Liu, Y. Q. Sun, Y. Y. Huo, H. X. Zhang, L. F. Wang, P. Zhang, D. Song, Y. W. Shi and W. Guo, *J. Am. Chem. Soc.*, 2014, **136**, 574.
5 Y. Zhang, Y. Li and X. P. Yan, *Anal. Chem.*, 2009, **81**, 5001–5007.
6 L. Y. Niu, Y. S. Guan, Y. Z. Chen, L. Z. Wu, C. H. Tung and Q. Z. Yang, *J. Am. Chem. Soc.*, 2012, **134**, 18928.
7 J. Yin, Y. Kwon, D. Kim, D. Lee, G. Kim, Y. Hu, J. H. Ryu and J. Yoon, *J. Am. Chem. Soc.*, 2014, **136**, 5351.
8 X. Chen, Y. Zhou, X. J. Peng and J. Yoon, *Chem. Soc. Rev.*, 2010, **39**, 2120.
9 B. Y. Han, J. P. Yuan and E. K. Wang, *Anal. Chem.*, 2009, **81**, 5569.
10 H. Huang, F. P. Shi, Y. A. Li, L. Niu, Y. Gao, S. M. Shah and X. G. Su, *Sens. Actuators, B*, 2013, **178**, 532.
11 M. Isik, T. Ozdemir, I. S. Turan, S. Kolemen and E. U. Akkaya, *Org. Lett.*, 2013, **15**, 216.
12 R. X. Peng, L. L. Lin, X. X. Wu, X. H. Liu and X. M. Feng, *J. Org. Chem.*, 2013, **78**, 11602.
13 H. Xu and M. Hepel, *Anal. Chem.*, 2011, **83**, 813.
14 Y. S. Guo, H. Wang, Y. S. Sun and B. Qu, *Chem. Commun.*, 2012, **48**, 3221.
15 P. K. Sudeep, S. T. S. Joseph and K. G. Thomas, *J. Am. Chem. Soc.*, 2005, **127**, 6516.
16 Z. P. Guan, S. Li, P. B. S. Cheng, N. Zhou, N. Y. Gao and Q. H. Xu, *ACS Appl. Mater. Interfaces*, 2012, **4**, 5711.
17 X. D. Liu, R. Sun, J. F. Ge, Y. J. Xu, Y. Xu and J. M. Lu, *Org. Biomol. Chem.*, 2013, **11**, 4258.
18 L. Zhou, Y. H. Lin, Z. Z. Huang, J. S. Ren and X. G. Qu, *Chem. Commun.*, 2012, **48**, 1147.
19 X. Ran, H. J. Sun, F. Pu, J. S. Ren and X. G. Qu, *Chem. Commun.*, 2013, **49**, 1079.
20 H. T. Li, Z. H. Kang, Y. Liu and S. T. Lee, *J. Mater. Chem.*, 2012, **22**, 24230.
21 P. J. G. Luo, S. Sahu, S. T. Yang, S. K. Sonkar, J. P. Wang, H. F. Wang, G. E. LeCroy, L. Cao and Y. P. Sun, *J. Mater. Chem. B*, 2013, **1**, 2116.

22 S. Y. Park, H. U. Lee, E. S. Park, S. C. Lee, J. W. Lee, S. W. Jeong, C. H. Kim, Y. C. Lee, Y. S. Huh and J. Lee, *ACS Appl. Mater. Interfaces*, 2014, **6**, 3365.
23 D. Y. Pan, J. C. Zhang, Z. Li and M. H. Wu, *Adv. Mater.*, 2010, **22**, 734.
24 L. L. Li, J. Ji, R. Fei, C. Z. Wang, Q. Lu, J. R. Zhang, L. P. Jiang and J. J. Zhu, *Adv. Funct. Mater.*, 2012, **22**, 2971.
25 X. Li, S. J. Zhu, B. Xu, K. Ma, J. H. Zhang, B. Yang and W. J. Tian, *Nanoscale*, 2013, **5**, 7776.
26 Y. Li, Y. Zhao, H. H. Cheng, Y. Hu, G. Q. Shi, L. M. Dai and L. T. Qu, *J. Am. Chem. Soc.*, 2012, **134**, 15.
27 G. S. Kumar, R. Roy, D. Sen, U. K. Ghorai, R. Thapa, N. Mazumder, S. Saha and K. K. Chattopadhyay, *Nanoscale*, 2014, **6**, 3384.
28 C. F. Hu, Y. L. Liu, Y. H. Yang, J. H. Cui, Z. R. Huang, Y. L. Wang, L. F. Yang, H. B. Wang, Y. Xiao and J. H. Rong, *J. Mater. Chem. B*, 2013, **1**, 39.
29 B. Song, C. D. B. Vandevyver, A. S. Chauvin and J. C. G. Bunzli, *Org. Biomol. Chem.*, 2008, **6**, 4125.
30 X. E. Jiang, C. Rocker, M. Hafner, S. Brandholt, R. M. Dorlich and G. U. Nienhaus, *ACS Nano*, 2010, **4**, 6787.
31 R. L. Arrowsmith, P. A. Waghorn, M. W. Jones, A. Bauman, S. K. Brayshaw, Z. Y. Hu, G. Kociok-Kohn, T. L. Mindt, R. M. Tyrrell, S. W. Botchway, J. R. Dilworth and S. I. Pascu, *Dalton Trans.*, 2011, 6238.
32 Y. Q. Dong, J. W. Shao, C. Q. Chen, H. Li, R. X. Wang, Y. W. Chi, X. M. Lin and G. N. Chen, *Carbon*, 2012, **50**, 4738.
33 J. Peng, W. Gao, B. K. Gupta, Z. Liu, R. Romero-Aburto, L. H. Ge, L. Song, L. B. Alemany, X. B. Zhan, G. H. Gao, S. A. Vithayathil, B. A. Kaipparettu, A. A. Marti, T. Hayashi, J. J. Zhu and P. M. Ajayan, *Nano Lett.*, 2012, **12**, 844.
34 Q. Xue, H. Huang, L. Wang, Z. W. Chen, M. H. Wu, Z. Li and D. Y. Pan, *Nanoscale*, 2013, **5**, 12098.
35 J. Ju and W. Chen, *Biosens. Bioelectron.*, 2014, **58**, 219.
36 R. Z. Zhang and W. Chen, *Biosens. Bioelectron.*, 2014, **55**, 83.
37 V. Gupta, N. Chaudhary, R. Srivastava, G. D. Sharma, R. Bhardwaj and S. Chand, *J. Am. Chem. Soc.*, 2011, **133**, 9960.
38 D. Qu, M. Zheng, P. Du, Y. Zhou, L. G. Zhang, D. Li, H. Q. Tan, Z. Zhao, Z. G. Xie and Z. C. Sun, *Nanoscale*, 2013, **5**, 12272.
39 V. Stengl, S. Bakardjieva, J. Henych, K. Lang and M. Kormunda, *Carbon*, 2013, **63**, 537.
40 L. L. Li, G. H. Wu, G. H. Yang, J. Peng, J. W. Zhao and J. J. Zhu, *Nanoscale*, 2013, **5**, 4015.
41 S. Q. Wang, Q. H. Wu, H. Y. Wang, X. X. Zheng, S. L. Shen, Y. R. Zhang, J. Y. Miao and B. X. Zhao, *Analyst*, 2013, **138**, 7169.
42 S. Y. Liu, F. P. Shi, L. Chen and X. G. Su, *Analyst*, 2013, **138**, 5819.